Phonon dispersion in transition metals

C. M. Varma and W. Weber*
Bell Laboratories, Murray Hill, New Jersey 07974
(Received 13 December 1978)

A new formulation of lattice dynamics especially suitable for transition metals and compounds is presented. Calculation of the phonon dispersion in 4*d* bcc metals and alloys based on it reproduce all the anomalies observed in inelastic-neutron-scattering experiments. The physical origin of the anomalies is discussed in detail.

I. INTRODUCTION

In recent years, inelastic neutron scattering experiments have revealed that the dispersion relations[1-3] for phonons in transition metals and compounds (TMC) have a very rich character. There are dips and peaks and wiggles in the phonon energy as a function of wave vectors in many TMC indicating that the atomic force constants have a very complicated distance and angular dependence.[4]

An understanding of the vibrational properties of TMC is well worth pursuing. Anomalies in the phonon dispersion signify incipient lattice instabilities. For instance, addition of Zr and Nb deepens the phonon anomaly in the longitudinal (111) branch in Nb, and ultimately at about $Zr_{0.8}Nb_{0.2}$ a structural transition to the ω phase results.[5] Many TMC prefer to form off-stoichiometry, and in complicated defect structures reflecting that on-stoichiometry and in simpler structures, the phonons' frequencies would be anomalous in peculiar places in the Brillouin zone. Metals and compounds with high superconducting transition temperature T_c—Nb and Ta and their alloys with Ti and Zr,[1-3] the group-VB transition-metal carbides and nitrides,[2] the layer transition-metal chalcogenides,[6] the high-T_c A-15 type compounds,[7] the Chevrel phases[8] and others—seem particularly afflicted with phonon anomalies. In fact the interest in understanding the coexistence of high-T_c and phonon anomalies has been a great impetus in the study of the lattice dynamics of TMC.[9]

A rigorous theory of the lattice dynamics[10] of metals is available and has been applied with considerable success to nearly-free-electron metals. Extensions of the same theory[11,12] to treat materials with rapidly varying charge density have been made, but they yield expressions complicated enough so that no realistic calculations based on them have to date been possible. In fact, starting with identical expressions, different authors[13,14] have come to widely varying conclusions about the physical mechanism of the anomalies depending on the difference in the models with which they evaluated them.

Empirical model calculations[15,16] have been successful in reproducing the phonon dispersions in some TMC, but the meaning of the parameters employed in such models is not clear in the context of the physics of metals.

In this paper, we present a new formulation of lattice dynamics especially suitable for calculations on materials with rapidly varying charge density such as the TMC. There are two equally important aspects of principle to this work. The first is the formulation itself in which we group the various terms in the dynamical matrix differently from that done in the usual formulation. This avoids many complications of the latter as we shall soon discuss. Second, we adopt the nonorthogonal tight binding (NTB) representation for the *d* electrons in finding an expression for the dynamical matrix. This avoids the difficulties and complications inherent in extensions of the augmented-plane-wave (APW) or Korringa-Kohn-Rostoker (KKR) representations—such as the rigidly moving muffin tin—to treat changes in electronic energy with lattice distortion.

We have found that the new formulation of lattice dynamics taking explicit cognizance of the tight-binding nature of the *d*-electron wave functions and using electron-phonon matrix elements calculated in a NTB basis set enables a realistic calculation of the phonon dispersion in a relatively simple fashion. We demonstrate this by comparing our calculations on the 4*d* bcc transition metals and alloys with experimental results. The use of the NTB method for electron phonon interactions leads to new insights into the role of electronic structure on phonons. In particular the prevalent view due originally to Kohn[17(a)] and Overhauser[17(b)] is found to need some revisions.

Our point of view on the tight-binding representation is foreshadowed by the work of Friedel[18] and collaborators, who over the years have con-

 © 1979 The American Physical Society

tinually emphasized the naturalness of tight-binding representation in TMC. The new lattice-dynamical formulation and the use of NTB in it was presented in a model calculation earlier.[9] Pickett and Gyorffy[19] at the same time presented the new formulation, but then represented the electronic structure in the phase shift formalism. This rendered the new formulation sufficiently complicated again that no realistic calculations have been performed with it. We shall compare the present work with those of the others in Sec. VI.

A brief account of this work has been published.[20]

II. DYNAMICAL MATRIX

The Hamiltonian for a system of electrons and ions is

$$H = T_e + T_c + V_{cc}(\{R\}) + V_{ee}(\{r\}) + V_{ec}(\{r\},\{R\}) . \tag{1}$$

In Eq. (1), T is the kinetic-energy operator, and V is the potential energy; the subscript c refers to the ion-cores and e to the valence electrons; $\{r\}$ denotes the electronic coordinates and $\{R\}$ the ion coordinates.

In the adiabatic approximation for the electron-ion system and the harmonic approximation to the effective ion-ion potential, the phonon frequencies $\omega_{q\lambda}$ (q : wave vector, λ : polarization) for a solid made up of one atom per unit cell are given by diagonalizing the dynamical matrix:

$$m\omega^2_{\vec{q}\lambda} = \epsilon^*_{\lambda\alpha}(\vec{q}) D_{\alpha\beta}(\vec{q})\, \epsilon_{\beta\lambda}(\vec{q}) , \tag{2}$$

$$D_{\alpha\beta}(\vec{q}) = \frac{1}{N}\sum_{i,j} D_{\alpha\beta}(\vec{R}_{ij}) \exp(i\vec{q}\cdot\vec{R}_{ij}) , \tag{3}$$

$$D_{\alpha\beta}(\vec{R}_{ij}) = \nabla_{i\alpha}\nabla_{j\beta}[V_{cc}(\{R\}) + E_e(\{R\})] . \tag{4}$$

In Eqs. (3)–(4), i,j label the lattice sites. $E_e(\{R\})$ is the total electronic energy, which in the adiabatic approximation depends parametrically on the configuration $\{R\}$ of the ions. Most of the problems in the lattice dynamics of metals arise in the proper treatment of $E_e(\{R\})$.

Our approach is to express $E_e(\{R\})$ in terms of the eigenvalues $\epsilon_{k\mu}$ (k : wave vector in the first Brillouin zone, μ : band index) of the self-consistent one-electron Hamiltonian. In the adiabatic approximation, the wave functions and the eigenvalues of the electrons are determined using the instantaneous configuration of the ions, $\{R\}$ in V_{ec}, as a parameter. In the one electron approximation, the two body term $V_{ee}(\{r\})$ is approximated in some self-consistent fashion to a one-body form. Because the wave function for the electrons depend parametrically on the instantaneous ionic configuration, so does the self-consistent electron-electron interaction; we denote the latter by $\overline{V}_{ee\{R\}}(\{r\})$. This interaction, $\overline{V}_{ee\{R\}}(\{r\})$, can be written as the sum of the Hartree potential and a one-body approximation to the correlation and exchange potential;

$$\overline{V}_{ee\{R\}}(\{r\}) = V^H_{\{R\}(\{r\})} + V^{xc}_{\{R\}}(\{r\}) , \tag{5}$$

$$V^H_{\{R\}}(\{r\}) = e^2 \int d^3r' \frac{\rho_{\{R\}}(\{r'\})}{|\vec{r}-\vec{r}'|} . \tag{6}$$

In Eq. (6), $\rho_{\{R\}}(\{r\})$ is the electronic density in a prescribed configuration of ions. There are various approximate schemes for V^{xc}, the most popular among these is to express it as a local functional[21] of the density $\rho(\{r\})$.

For the configuration in which the ions are at the equilibrium lattice sites, one can introduce the wave-vector index k in the first Brillouin zone and the band index μ as quantum numbers for the electronic wave function so that the one-electron Schrödinger equation for the electrons is

$$(T_e + V_{ec} + V_{ee})\psi_{\vec{k}\mu} = \epsilon_{\vec{k}\mu}\psi_{\vec{k}\mu} , \tag{7}$$

where we have omitted the labels $\{r\},\{R\}$ for simplicity.

We wish to express E_e in terms of the self-consistent eigenvalues $\epsilon_{\vec{k}\mu}$. Towards this end, we first define

$$E_\Sigma = \sum_{\vec{k}\mu} \epsilon_{\vec{k}\mu} f(\vec{k}\mu) , \tag{8}$$

where $f(\vec{k}\mu)$ is the Fermi function. E_Σ is the sum of the energies of the occupied electronic states. In obtaining $\epsilon_{\vec{k}\mu}$, the two-body electron-electron interaction terms have been approximated by one-body terms. Therefore E_Σ includes the interaction energy twice. The total electronic energy E_e is

$$E_e = E_\Sigma - \langle \overline{V}_{ee} \rangle ; \quad \langle \overline{V}_{ee} \rangle = \langle V^H \rangle + \langle V^{xc} \rangle , \tag{9}$$

where $\langle\ \rangle$ denotes the expectation value. Thus

$$\langle V^H\{R\} \rangle = \tfrac{1}{2} e^2 \int d^3r \int d^3r' \frac{\rho_{\{R\}}(r)\rho_{\{R\}}(r')}{|\vec{r}-\vec{r}'|} . \tag{10}$$

Now we define

$$V_0(\{R\}) \equiv V_{cc}(\{R\}) - \langle \overline{V}_{ee}(\{R\}) \rangle , \tag{11}$$

and the contribution of V_0 to the dynamical matrix,

$$D^{(0)}_{ij} \equiv \nabla_i \nabla_j V_0 . \tag{12}$$

The remaining contribution to the dynamical matrix arises from $E_\Sigma(\{R\})$.

In Eq. (9), $\langle V^{xc}\{R\} \rangle$ is a short-range function of the distance between the ions, and the long-range Coulomb term in V_{cc} is exactly cancelled by V^H for a metal with one atom per unit cell. $V_{cc} - V^H$ is also much smaller than either V_{cc} or V^H. This cancellation is better the more tightly bound the atomic orbitals are. We note that by express-

ing the dynamical matrix, Eq. (3), in terms of V_0 and E_Σ, one of the major problems of the customary approach is overcome. In that approach V_{cc} and E_e are separately calculated and the cancellation that we have explicitly considered to begin with in Eq. (9), is brought about by a complicated treatment of E_e.

Next, consider the contribution of E_Σ to the dynamical matrix: $\nabla_i \nabla_j E_\Sigma(\{R\})$. To evaluate this term, we must consider the shift in the eigenvalues $\epsilon_{\vec{k}\mu}$ as the ions are perturbed from the equilibrium lattice sites. There are two contributions to the dynamical matrix due to the perturbation: $D^{(1)}$ due to first-order corrections to $\epsilon_{\vec{k}\mu}$ arising from second-order displacements, and $D^{(2)}$ due to second-order corrections to $\epsilon_{\vec{k}\mu}$ arising from first-order displacements.

To evaluate $D^{(2)}$ we need the matrix element $g^{\alpha}_{\vec{k}\mu,\vec{k}'\mu'}$ for scattering of a state $\vec{k}\mu$ to a state $\vec{k}'\mu'$ as the ions are moved in the αth Cartesian direction in a periodic wave of wave vector $\vec{q}=\vec{k}-\vec{k}'$. Since $\overline{V}_{ee}$ in Eq. (7) depends parametrically on $\{R\}$ through its dependence on the wave functions $\psi_{\vec{k}\mu}$, the matrix element $g^{\alpha}_{\vec{k}\mu,\vec{k}'\mu'}$ must be self-consistent (or renormalized) in that it should take into account the variation in $\overline{V}_{ee}$ with lattice displacement.

Since no wave-function change is involved in $D^{(1)}$, it should be calculated from variations in $\epsilon_{\vec{k}\mu}$ arising merely from variations in V_{ee} with displacement of ions.

III. TIGHT-BINDING REPRESENTATION OF THE ELECTRONIC CONTRIBUTION TO THE DYNAMICAL MATRIX

We have found it most convenient to adopt the tight-binding representation for electrons in TMC in deriving expression for D_1 and D_2. For tight binding to be a good physical representation, one must take account of the nonorthogonality of the atomic orbitals. The quantitative validity of this approach has been established[22] by the good agreement with experimental results obtained in a calculation of $\langle I^2\rangle$, the squared average of electron-phonon scattering on the Fermi surface.

In NTB the Bloch functions are

$$\psi_{\vec{k}\mu}=\frac{1}{\sqrt{N}}\sum_{i,m}\exp(i\vec{k}\cdot\vec{R}_i)A_{\mu m}(\vec{k})\phi_{im}(\vec{r}), \tag{13}$$

where $\phi_{im}(\vec{r})$ is the localized orbital with quantum number m at site i, and A satisfies

$$HA=SAE, \tag{14}$$

with normalization

$$A^{\dagger}SA=I. \tag{15}$$

In Eq. (14), H is the Hamiltonian matrix, and S is the overlap matrix. It is important to note that Eq. (14) is regarded here as completely equivalent to Eq. (7); thus the matrix elements of H and S are self-consistent quantities including the effect of the electron-phonon interactions. For details of our use of the NTB method, please see Ref. 22, hereafter referred to as I.

The change in an eigenvalue $\epsilon_{\vec{k}\mu}$ as H and S is varied by δH and δS, respectively, can easily be found. To second order in the perturbation

$$\delta\epsilon_{\vec{k}\mu}=\delta\epsilon^{(1)}_{\vec{k}\mu}+\delta\epsilon^{(2)}_{\vec{k}\mu}, \tag{16}$$

$$\delta\epsilon^{(1)}_{\vec{k}\mu}=\sum_{m,n}A^{\dagger}_{\mu m}(\vec{k})[\delta H_{mn}(\vec{k})-\epsilon_{\vec{k}\mu}\delta S_{mn}(\vec{k})]A_{n\mu}(\vec{k}), \tag{17}$$

$$\delta\epsilon^{(2)}_{\vec{k}\mu}=-\sum_{\substack{\vec{k}',\mu'\\ m,n}}A^{\dagger}_{\mu m}(\vec{k})[\delta H_{mn}(\vec{k})-\epsilon_{\vec{k}\mu}\delta S_{mn}(\vec{k})]A_{n\mu'}(\vec{k}')A^{\dagger}_{n\mu'}(\vec{k}')[\delta H_{nm}(\vec{k}')-\epsilon_{k\mu}\delta S_{nm}(\vec{k}')]A_{m\mu}(\vec{k}),$$
$$\times(\epsilon_{\vec{k}\mu}-\epsilon_{\vec{k}'\mu'})^{-1}[1-f(\vec{k}'\mu')]. \tag{18}$$

In our numerical calculations of D_2 we have used the two center approximation and ignored the (small) variation in the crystal-field integrals due to ion motion. With these approximations, we can write

$$\delta H_{im,jn}=\nabla H_{im,jn}\cdot(\vec{u}_i-\vec{u}_j)+\tfrac{1}{2}(\vec{u}_i-\vec{u}_j)\cdot\nabla^2 H_{im,jn}\cdot(\vec{u}_i-\vec{u}_j), \tag{19}$$

$$\delta S_{im,jn}=\nabla S_{im,jn}\cdot(\vec{u}_i-\vec{u}_j)+\tfrac{1}{2}(\vec{u}_i-\vec{u}_j)\cdot\nabla^2 S_{im,jn}\cdot(\vec{u}_i-\vec{u}_j). \tag{20}$$

As discussed in I, ∇H and ∇S are to be interpreted as renormalized parameters including the effect of the variation of electron-electron interactions with displacement of atoms.

With Eqs. (19)–(20) it is straightforward to derive expressions for $D^{(1)}$ and $D^{(2)}$. We find

$$D^{(1)}_{\alpha\beta}(\vec{q})=\frac{1}{2}\sum_{\vec{k}\mu,n,m,\vec{R}_{ij}}A^{\dagger}_{\mu n}(\vec{k})(\nabla_\alpha\nabla_\beta H_{in,jm}-\epsilon_{\vec{k}\mu}\nabla_\alpha\nabla_\beta S_{in,jm})A_{\mu m}(\vec{k})\times\exp(i\vec{q}\cdot\vec{R}_{ij})f(\vec{k}\mu), \tag{21}$$

and

$$D^{(2)}_{\alpha\beta}(\vec{q}) = -\sum_{\vec{k}\mu,\mu'} \frac{g^{\alpha *}_{\vec{k}\mu,\vec{k}+\vec{q}\mu'} g^{\beta}_{\vec{k}+\vec{q}\mu',k\mu}[f(\vec{k}\mu) - f(\vec{k}+\vec{q}\mu')]}{\epsilon_{\vec{k}\mu} - \epsilon_{\vec{k}+\vec{q}\mu'}}, \tag{22}$$

where

$$g^{\alpha}_{\vec{k}\mu,\vec{k}'\mu'} = \sum_{m,n} A^{*}_{\mu m}(\vec{k}) \times\{[\gamma^{\alpha}_{mn}(\vec{k}) - \gamma^{\alpha}_{mn}(\vec{k}')] - \epsilon_{\vec{k}\mu}[\sigma^{\alpha}_{mn}(\vec{k}) - \sigma^{\alpha}_{mn}(\vec{k}')]\} A_{n\mu}(\vec{k}'), \tag{23}$$

$$\gamma^{\alpha}_{mn}(\vec{k}) = \sum_{\vec{R}_{ij}} \nabla H_{im,jn} \exp(i\vec{k}\cdot\vec{R}_{ij}), \tag{24a}$$

$$\sigma^{\alpha}_{mn}(\vec{k}) = \sum_{\vec{R}_{ij}} \nabla S_{im,jn} \exp(i\vec{k}\cdot\vec{R}_{ij}), \tag{24b}$$

is the renormalized electron-phonon matrix. For elastic scattering the same quantity had been derived in I from time-dependent perturbation theory.[22]

IV. COMPARISON WITH THE INVERSION APPROACH

The usual method in the theory of lattice dynamics metals[10] is to calculate the dynamical matrix, Eq. (3) directly from V_{cc} and E_e. If electron-electron interactions are ignored the change in E_e with displacement of ions is as shown in Fig. 1(a) and is given by

$$\delta E_e = g_0 \chi_0 g_0, \tag{25}$$

where g_0 is the bare electron-phonon interaction and χ_0 is the electronic susceptibility. To include the effect of the electron-electron interactions, χ_0 in Eq. (25) must be replaced by a renormalized susceptibility; for instance in random-phase approximation (RPA), δE_e is given by

$$\delta E_e^{\mathrm{RPA}} = g_0 \chi g_0 = g \chi_0 g_0$$
$$\chi = \epsilon^{-1}\chi_0, \tag{26}$$

where ϵ is the dielectric constant. $\delta E_e^{\mathrm{RPA}}$ is shown in Fig. 1(b). The inversion of ϵ in Eq. (27) is a very formidable problem for materials with rapidly varying change density. It must be done very accurately to properly represent the local field effects and thereby to correctly screen the Coulomb interaction V_{cc}; in the plane-wave method several hundred waves are required to represent the charge density for such materials. This means the matrix ϵ is enormous. Localized representations to handle this problem have been derived,[11,12] but for a bcc transition metal ϵ must still be a 135×135 matrix in general, to take into account nearest- and next-nearest-neighbor overlaps. There is also considerable difficulty in these methods in finding the bare vertex g_0. The approximation of rigidly moving muffin tin may be used but it is an uncontrolled approximation.

In $D^{(2)}$ in Eq. (22), we calculate $g\chi_0 g$, which is represented in Fig. 1(c). But as shown in Fig. 1(d), $g\chi_0 g$ is equal in RPA to $D^{(2)} - \langle\nabla\nabla\nabla^H\rangle$. We have explicitly considered $\langle\nabla\nabla\nabla^H\rangle$ in $D^{(0)}$ by Eq. (12). Thus, the two methods are formally equivalent in RPA. This equivalence can be shown more generally.[23]

Besides the obvious advantage of working with V_0 rather than V_{cc}, the method presented in this paper has several computational advantages: (i) The changes in the Hamiltonian due to ion motion are expressed in terms of derivatives of matrix elements taken at discrete lattice points i, j, etc. Thus we do not explicitly require the knowledge of the wave functions and potential gradients at all points in space and yet include local field effects. (ii) The effect of variation in screening, exchange and correlations is included in the terms ∇H_{ij}, ∇S_{ij}, as long as these quantities are determined from self-consistent band structure calculations at different lattice configurations. (iii) The significant ∇H_{ij} and ∇S_{ij} are confined to a few nearest neighbors. All this makes the calculations

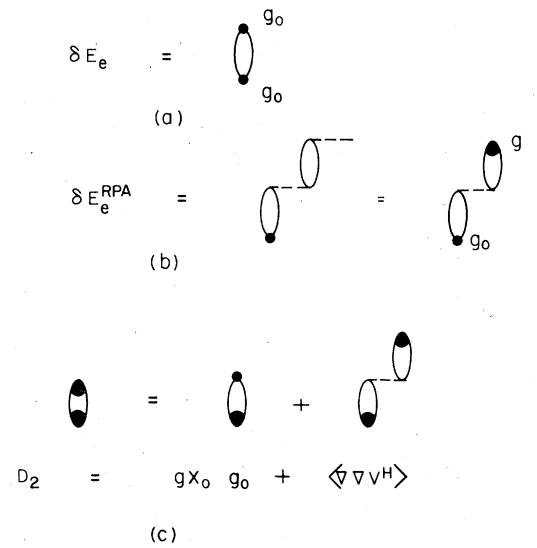

FIG. 1. Equivalence of the present method of calculating the dynamical matrix to the traditional method is shown within RPA.

economical without introducing any uncontrolled approximations.

An additional bonus, which is obvious from the form of Eq. (24), is that the wave-vector dependence of the matrix element is given correctly provided only that the ratios of ∇H and ∇S for the first few neighbors is given accurately.

The conceptual advantage of working in the tight-binding representation is that we are able to express the electron-phonon matrix elements in terms of the features of the electronic structure. This, as we shall soon show, sheds new insight into the role of Fermi-surface topology on phonon dispersion.

V. METHOD OF CALCULATION

It is easy to see that the range of the force constants in $D^{(1)}$ is the same as the range of the matrix elements H_{ij} and of the overlap elements S_{ij}. The long-range effects in $D^{(0)}$ arising from scattering near the Fermi surface can be shown to be much smaller than those in $D^{(2)}$.[23] Since we are primarily interested in this paper in the anomalous features of the phonon spectrum, and since these cannot arise from short-range force constants, we do not attempt a calculation of $D^{(0)}+D^{(1)}$. Instead we parametrize it by nearest- and next-nearest-neighbor force constants. In a cubic crystal this introduces four parameters. They are determined so that the diagonalization of $D^{(0)}+D^{(1)}+D^{(2)}$ yields best agreement with the experimentally determined phonon dispersion curves. The short-range parameters for Nb, Mo, and some of their alloys are given in Table I. They are smoothly varying, in general increasing with e/a ratio.

We calculate $D^{(2)}$ from first principles. This requires a knowledge of the band structure, the Fermi surface, the eigenvectors $A_{m\mu}(\vec{k})$, and the matrix elements $g^{\alpha}_{\vec{k}\mu,\vec{k}+\vec{q}\mu'}$. The same quantities are required in the calculation of $\langle I^2\rangle$, the average-squared electron-phonon matrix element on the Fermi surface. Since these quantities have been evaluated for the bcc transition metals in I, and a detailed discussion of their evaluation has been given, we do not repeat it here. The excellent agreement of the calculated $\langle I^2\rangle$ with the experimentally deduced result gives us confidence in the method of evaluation and of the efficacy of the NTB method for quantitative calculations. Since the phonon anomalies arise from $D^{(2)}$ which just as $\langle I^2\rangle$ is determined without any adjustable parameters, we have confidence also in the conclusions we draw regarding the origin of the anomalies.

We briefly summarize the method of evaluation of $D^{(2)}$. The NTB band structure with a nine-orbital s-p-d basis is fitted to APW calculations[24] for Nb with a rms error of ≈0.15 eV. The NTB matrix elements extend to second neighbors, and the two-center approximation is used. The NTB band structure is shown in Fig. 2 and the corresponding density of states is depicted in Fig. 3. The radial derivatives in ∇H and ∇S are determined from (i) fits to self-consistent APW band-structure calculations[25] at two different lattice constants and (ii) Herman-Skillman atomic wave functions and potentials. The two methods lead to results which agree within ≈20%. The atomic wave functions and potentials of Herman-Skillman are

TABLE I. Short-range force constants (10^4 dynes/cm) for various electron/atom ratios. Born and von Karman ($1nn$ and $2nn$) force constants (in eV/A^2) representing D_0+D_1. For convenience we recall the definition of the force-constant matrices: $F^{1nn}_{xy}=\alpha\delta_{xy}+\beta(1-\delta_{xy})$; $F^{2nn}_{xx}=A$; $F^{2nn}_{yy}=F_{zz}=B$; $F^{2nn}_{xy}=0$.

Electron/atom	α	β	A	B
5.0	7.04	1.28	1.48	1.62
5.20	7.33	1.37	1.73	1.87
5.40	7.50	1.47	1.84	2.08
5.75	8.34	1.42	1.75	2.40
6.0	8.73	1.25	2.63	2.38

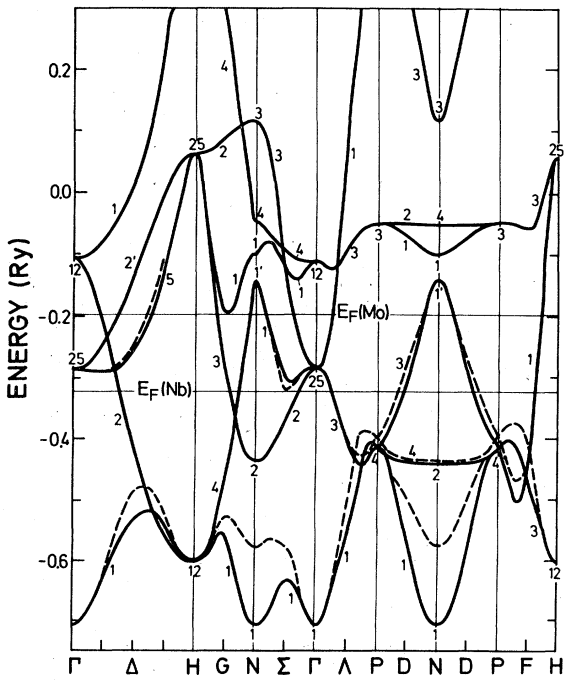

FIG. 2. NTB band structure (fitted to that in Ref. 26) used for Nb, Mo, and their alloys. Where the first principles band structure (Ref. 24) visibly deviates from the NTB band structure, is shown as a dashed line.

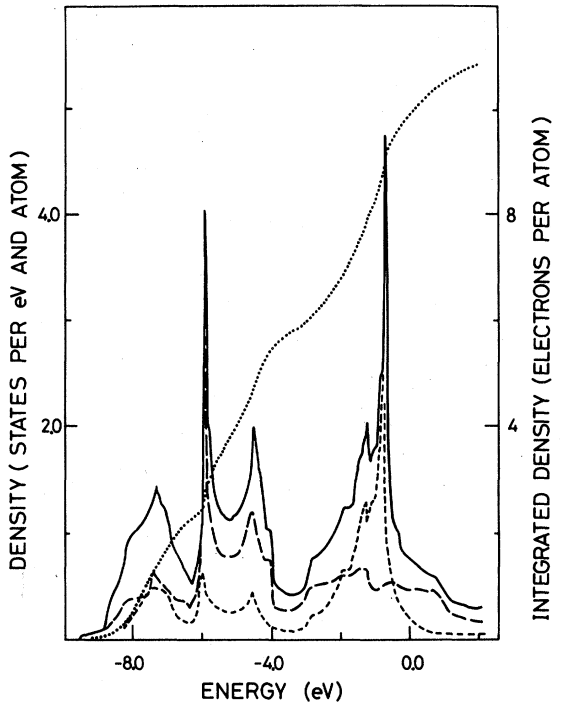

FIG. 3. Density of states and integrated density of states for Nb, Mo, and their alloys. The e_g density of states (short dashes) and the t_{2g} density of states (long dashes) are also shown.

self-consistent quantities including the effects of intra-atomic exchange and correlations by the $\rho^{1/3}$ approximation. Our finding that the parameters H, S, and $\nabla H, \nabla S$, determined by methods (i) and (ii), differ only by about 20% implies that *inter-atomic* exchange and correlations are corrections to these parameters of utmost about 20%.

The principal value integral in $D^{(2)}$ is calculated using the method and the program of Diamond.[26] Here the Brillouin zone (BZ) is divided into little cubes and the energy $E(k)$ in such a cube is linearly approximated. With this approximation, the expression

$$\int_{\vec{k}'=\vec{k}+\vec{q}}^{\text{cube}} d^3k \frac{f_{\vec{k}}-f_{\vec{k}'}}{E_{\vec{k}}-E_{\vec{k}'}} \tag{27}$$

is calculated exactly by Diamond's program. In this method the integration is performed by defining a mesh of cubes. We found it most convenient to choose the cube centers at $(2\pi/a)(1/2n)(h, k, l)$, with h, k, l being odd integers, and n is the number of cubes along the line Γ-H. (Cubes extending into other BZ's have been weighted according to their volume in the first BZ.) This choice of the mesh allows us to calculate phonons of the wave vector

$$\vec{q} = (2\pi/a)(1/2n)(h', k', l'),$$

with h', k', l' being even integers. Thus with n cubes along Γ-H, phonons with n different q values along this line can be calculated.

The matrix elements $g^{\alpha}_{k\mu,k'\mu'}$ are evaluated at the cube centers. Their k dependence within the cube is ignored. This approximation is not always very good, as we sometimes find rather rapidly varying matrix elements.

We have examined the convergence of this method by using various meshes and have found good convergence for $n=8$ and $n=10$ (corresponding to 40 and 70 cubes, respectively, in the small ($\frac{1}{48}$ BZ) in almost all cases. Only for the intraband contribution to the N_3' phonon in Mo and Mo-rich alloys, the convergence was not quite satisfactory even with $n=16$ (=240 cubes). In this case we are faced with very rapidly varying matrix elements.

$D^{(2)}$ has been calculated for Nb, Mo, and a few Nb-Mo alloys in a "transium" model; i.e., a rigid-band structure has been used and only the Fermi energy E_F and the lattice constant (as well as the atomic mass) have been varied. The "transium" model is supported by various results, among which we may mention the very good agreement of the electronic density of states curve with the specific heat data of Nb-Mo alloys,[27] the strong similarity of Nb and Mo band structures,[28] and the coherent-potential approximation (CPA) calculations for Nb-Mo alloys.[29] All these results indicate that the force constant fluctuations in the alloys are small; in addition, the mass fluctuations are very small. We also note that Powell *et al.*[1] did not observe any increased widths of the neutron groups in the alloys.

VI. RESULTS AND DISCUSSION

A. Phonon anomalies

The phonon dispersion curves for Nb, $Nb_{0.8}Mo_{0.2}$, $Nb_{0.6}Mo_{0.4}$, $Nb_{0.25}Mo_{0.75}$, and Mo are shown in Figs. 4–8. We note that all anomalous features in these curves are correctly reproduced. These are, for Nb, along $(\xi, 0, 0)$, the dip in the longitudinal (L) branch near $\xi = 0.7$, along (ξ, ξ, ξ), the very deep minimum in L near $\xi = 0.7$, and the kink in L near 0.4. Also reproduced are the negative curvatures in the transverse (T) branches in $(\xi, 0, 0)$ and $(\xi, \xi, 0)$ including the very small value of c_{44} and the crossing of the two T branches in $(\xi, \xi, 0)$.

When going toward Mo-rich alloys all the anomalous features in the dispersion curves fade away (see Figs. 5 and 6) and disappear around $Nb_{0.25}Mo_{0.75}$ (see Fig. 7). Near Mo (see Fig. 8) completely new features appear. The most dram-

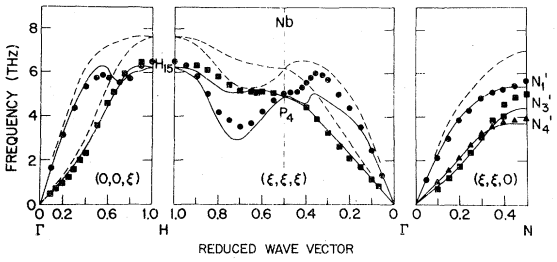

FIG. 4. Calculated dispersion curve for Nb compared with experiments, Ref. 1. Dashed curves are the dispersion curves obtained if $D_2^<$ is omitted.

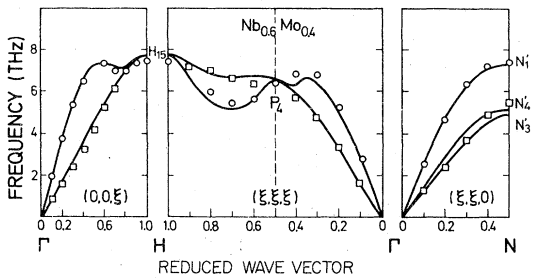

FIG. 6. Calculated dispersion curve for $Nb_{0.6}Mo_{0.4}$ compared with experiments, Ref. 1.

atic is the strong softening of the phonons around the H point, and the crossing of L and T branches near $\xi = 0.9$ in (ξ, ξ, ξ). Similarly, one T branch in $(\xi, \xi, 0)$ near N, especially the N_3' mode starts to decrease rapidly.

B. Analysis of the anomalies

We have carefully analyzed our calculations to trace the source of the anomalies and the nature of the overall spectrum. We find that almost all anomalous features in the dispersion curves of Nb, Mo, and the Nb-Mo alloys arise from scattering processes in $D^{(2)}$ with energies $E_{k\mu}$ and $E_{k'\mu'}$ close to E_F, approximately in the range ± 0.5 eV. The concave curvature in the T branches of Nb is the only exception to this finding (see discussion below).

The importance of small-energy scattering in $D^{(2)}$ is demonstrated in Fig. 4 (Nb) and Fig. 8 (Mo). When the contributions $D_2^<$ of states $\approx \pm 0.5$ eV around the Fermi energy are omitted in D_2 all the anomalous structure is absent. It should be noted that in Nb and Nb-rich alloys $D_2^<$ is equivalent to intraband scattering of band 3 (counted from the bottom, see Fig. 2). For Nb this band yields $\approx 90\%$ of $N(E_F)$. In Mo, $D_2^<$ stems from interband scattering between bands 3 and 4. The various contributions to $D^{(2)}$ for Nb are also illustrated in Fig. 9. In a first step, all band 3 interband scattering, i.e., $D_2^<$ is omitted. Here the negative curvature of the long wavelength T branches is still present. In a second step we also omit all scattering within the lowest six bands which are mainly d-like. Now the negative curvature has also disappeared. The rest of $D^{(2)}$ scattering from the d-like bottom to the p-like top of the band complex with an average gap of ≈ 10 eV is completely structureless, hence the phonon curves show very smooth behavior indicative of very short-range force constants.

Thus all structure in the dispersion curves originates from D_2^{d-d}, the scattering within the mainly d-like bands. In these bands, the wave functions have only 10%–15% s- or p-like character. We have found that s-d or p-d scattering is unimportant mainly because of the small admixture of s and p orbitals, and to a lesser extent because they have smaller gradients ∇H_{ij}^{mn} (see Table I of I). An analysis of the relative importance of the various coupling gradients ∇H shows that $dd\sigma$ ($1nn$ and $2nn$) and $dd\pi$ ($1nn$) dominate in D_2^{d-d}, all other matrix elements contribute less than 10%. The uncertainties in determining the less important coupling gradients (for instance those involving the s orbitals) are therefore of little consequence for our results. A variation of the magnitude of the d-d gradients causes a change in the magnitude of D_2, but the q dependence of $D^{(2)}$ is not significantly altered. Similarly, the omission of the

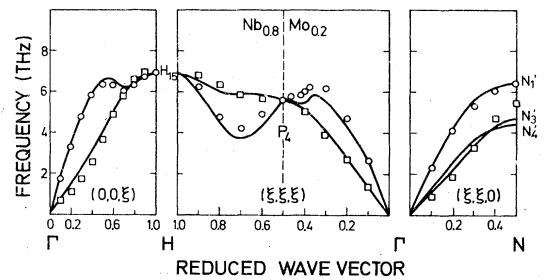

FIG. 5. Calculated dispersion curve for $Nb_{0.8}Mo_{0.2}$ compared with experiments, Ref. 1.

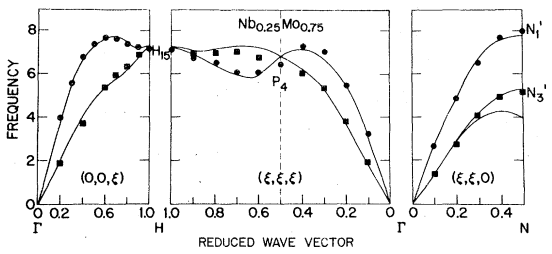

FIG. 7. Calculated dispersion curve for $Nb_{0.25}Mo_{0.75}$ compared with experiment, Ref. 1.

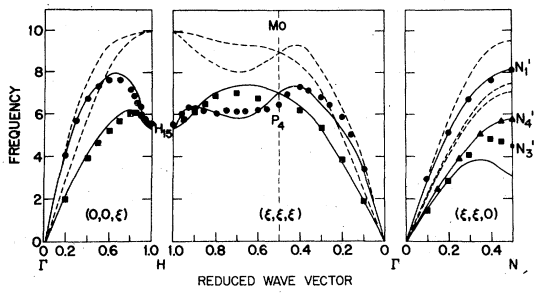

FIG. 8. Phonon-dispersion curves for Mo. Solid lines show our calculation; the symbols denote the experimental values of Ref. 6. The dashed lines show our results excluding D_2^{ζ}, which corresponds to excluding band 3–4 and 3–5 transitions (counted from bottom).

∇S term in $g^{\alpha}_{k\mu,k'\mu'}$ only leads to an increase of $D^{(2)}$ but does not change its q dependence.

The negative curvature of the T branches is caused by large $D^{(2)}(T)$ at long wavelengths due mainly to scattering from band 2 to band 4, around the N point. Here the average $\Delta E_{kk'} \approx 4$ eV. As compared to the other structures, the T anomaly extends rather far in q space, approximately between $0 \leq \xi < 0.6$ along Γ-H. Also the result $D_2(T)/D_2(L) \approx 2$ near $\xi \approx 0$ is found both for Nb and Mo and the Nb-Mo alloys. Therefore the ratio $c_{11}/c_{44} \gg 1$ in all materials (in a 1nn force constant model for the bcc structure we would obtain $c_{11} = c_{44}$). We should also note that though any fit of the 1nn and 2nn force constants representing $D_0 + D_1$ yields large c_{11}/c_{44} ratios, a visible negative curvature in Nb is only achieved by weighing the T phonons somewhat stronger than the others.

We now discuss in detail the anomaly in the L branch of Nb at $q_a \approx (0, 0, 0.7)$, which is representative for all L anomalies in Nb. Consider the energy vs wave-vector plane of band 3 (see Fig. 10). The Fermi surface forms a "jungle-gym" with the junctions of the interpenetrating rods at the Γ and H points. Other pieces of the Fermi surface form "islands" around the N points. The strongest contributions by far to D_2^{ζ} come from the region $k \approx (0.15,\ 0.45 \pm \delta,\ 0.1 \pm \epsilon)$ with $\delta \approx 0.15$ and $\epsilon \approx 0.05$, and the corresponding $\vec{k} + \vec{q}_a$ region, as indicated in Fig. 10. The two areas have almost parallel pieces of the Fermi surface with nesting vector q_a. This means that for this scattering, a relatively large phase space of states k and $k + q_a$ around E_F is available. It is, however, misleading to look just for nesting of states E_k and E_{k+q} with favorably small energy differences. This is seen from a calculation of the "bare" intraband susceptibility

$$\chi_{33}(\vec{q}) = \sum_{\substack{\vec{k},\vec{k}'=\vec{k}+\vec{q} \\ \mu=\mu'=3}} (f^{\mu}_{\vec{k}} - f^{\mu'}_{\vec{k}'})/(E^{\mu}_{\vec{k}} - E^{\mu'}_{\vec{k}'}) , \tag{28}$$

which corresponds to $g_{kk'} = \text{const}$. From an expansion of the denominator in Eq. (28),

$$(E^{\alpha}_{\vec{k}} - E^{\alpha}_{\vec{k}'}) = \Delta E_0 + (v^{\alpha}_{k_0} - v^{\alpha}_{k'_0})(k^{\alpha} - k^{\alpha}_0) , \tag{29}$$

we would expect a maximum in $\chi(\vec{q})$ for $\Delta E_0 \approx 0$ and $v^{\beta}_k \approx v^{\beta}_{k'}$; i.e., for parallel or dispersionless bands. $\chi_{33}(\vec{q})$ along $(0, 0, \xi)$ shows a maximum near

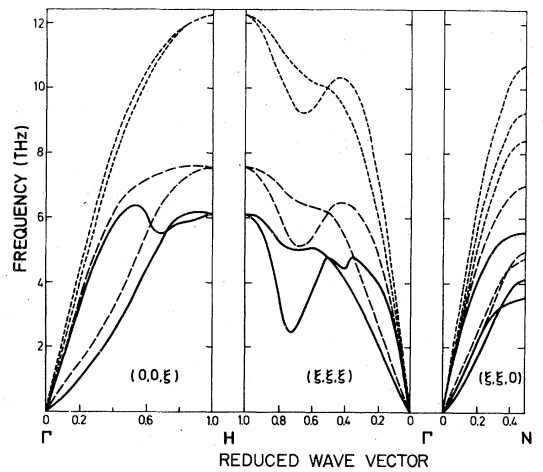

FIG. 9. Phonon-dispersion curves for Nb calculated using (i) complete D_2 (full lines), (ii) omitting band 3 intraband scattering in D_2 (long-dashed lines) and (iii) omitting all scattering within bands 1–6, which are mainly d-like bands (short-dashed lines).

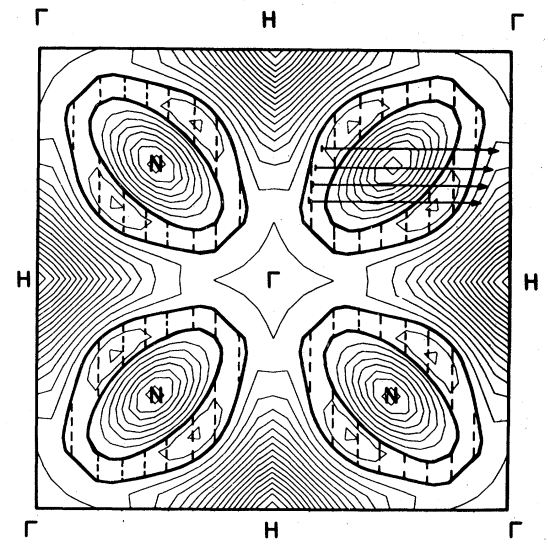

FIG. 10. Contour plot of the band 3 energy of wave-vector plane. The coordinates are the k_x and k_y directions; $k_z = 0.06$. The E_F contour lines are specially marked. All areas below E_F are indicated by hatching. Also shown is the scattering area around $k_x = 0.15$, $k_y = 0.45 \pm 0.02$ which yields the largest contributions to D_2^{ζ}.

$q \approx 0.5$, but actually has a minimum for $q_a = 0.7$ (see Fig. 2 of Ref. 20). Also along (ξ, ξ, ξ) the structure in $\chi_{33}(\vec{q})$ does not coincide with peaks in $D_2^<(L)$. On the other hand, if the q dependence of the energy denominators is ignored in the calculation of $D_2^<$ by replacing it with $N(\epsilon_F)$, and

$$N(\epsilon_F) \sum_k |g^{\alpha}_{\vec{k},\vec{k}+\vec{q}}|^2 f_{\vec{k}}(1 - f_{\vec{k}+\vec{q}}) \tag{30}$$

is plotted (see Fig. 2 of Ref. 20, the anomalous features of the true $D_2^<(q)$ are qualitatively reproduced).

It is therefore clear that the phonon anomalies have to do with the q dependence of the electron-ion form factors $g^{\alpha}_{\vec{k},\vec{k}+\vec{q}}$. The physical origin of the anomalies and the difference with the traditional view are best illustrated if we use the approximation for $g^{\alpha}_{k\mu,k+q\mu'}$, derived in I

$$g^{\alpha}_{\vec{k}\mu,\vec{k}'\mu'} \sim (v^{\alpha}_{\vec{k}\mu} - v^{\alpha}_{\vec{k}'\mu'}) \sum_m A^*_{\mu m}(\vec{k}) A_{\mu' m}(\vec{k}), \tag{31}$$

where $v^{\alpha}_{k\mu}$ is the velocity $\partial \epsilon_{k\mu}/\partial_{k\alpha}$. The phonon anomalies arise because lattice distortions at certain wave vectors cause a relatively large change in the electronic energy, and it is precisely this variation that we are calculating in $D^{(2)}$ (and $D^{(1)}$). The reduction in energy can obviously be most significant if local gaps in the electronic structure open up at the Fermi surface for certain lattice distortions. Inserting (31) in Eq. (22) for $D^{(2)}$, we conclude that a lattice distortion of wave vector $q = k - k'$ will reduce the energy of a state $k\mu$ near the Fermi surface significantly if a state $k'\mu'$ near the Fermi surface exists such that $|v^{\alpha}_{k\mu} - v^{\alpha}_{k'\mu'}|$ is large. The anomaly will appear in the longitudinal mode for α parallel to q and in the transverse modes for α orthogonal to q. This effect is proportional to $|v^{\alpha}_{k\mu} - v^{\alpha}_{k'\mu'}|^2$, while the number of states $k\mu$ near the Fermi surface is $\sim |v_{k\mu}|^{-1}$. Only the latter effect is present in the usual Kohn-Overhauser theory, so that for nesting of bands near the Fermi surface, it predicts phonon anomalies for small $|v^{\alpha}_{k\mu}|$, whereas we predict phonon anomalies for large $|v^{\alpha}_{k\mu}|$. In the above discussion α is the nesting direction. In D_2 one must integrate over the other two components of the wave vector also. To get a large effect from these, only the energy denominator is relevant. For the energy denominator to be as small as possible, the initial and final bands in the scattering process must be nearly parallel. This is generally likely if the bands are flat in these directions. We therefore conclude that materials with sharp saddle points in the band structure near the Fermi surface give rise to the largest phonon anomalies.

We reiterate that these effects are not present merely in the $\chi_0(q)$. The sharpness of the saddle point [large $(v^{\alpha}_{k\ \text{initial}} - v^{\alpha}_{k\ \text{final}})$] washes away the q dependence in the $\chi_0(q)$ for Nb etc., but makes it very prominent in $D^{(2)}$. This need not always be so. For NbC, Gupta and Freeman,[30] and Klein *et al.*[31] have found peaks in $\chi_0(q)$ from scattering within a band near the Fermi surface at the places of the anomalies. Calculations in NbC of $D^{(2)}$ (which will be published separately), however, enhance these peaks by an order of magnitude.

To exhibit the relationship of the anomalies to the electronic dispersion even more clearly we consider the functions

$$E_1(x) = E_{\mu=3}(k^0_x + x, k^0_y, k^0_z) \tag{32}$$

and

$$E_2(x) = E_{\mu=3}(k^0_x + q + x, k^0_y, k^0_z) \tag{33}$$

with $k^0 = (0.15,\ 0.45,\ 0.05)$ and $0 \leq x \leq 2$. A typical wave vector is k_0 from the region of largest contribution to $D_2^<$. We first choose $q = q_a = 0.7$ [see Fig. 11(b)]. Here E_1 and E_2 run completely out of phase; the band velocities are large and of opposite sign whenever E_1 and E_2 cross each other. For $q = 0.5$ [see Fig. 11(a)], E_1 and E_2 run almost parallel and generally at points where they cross, the band velocities have the same sign and almost the

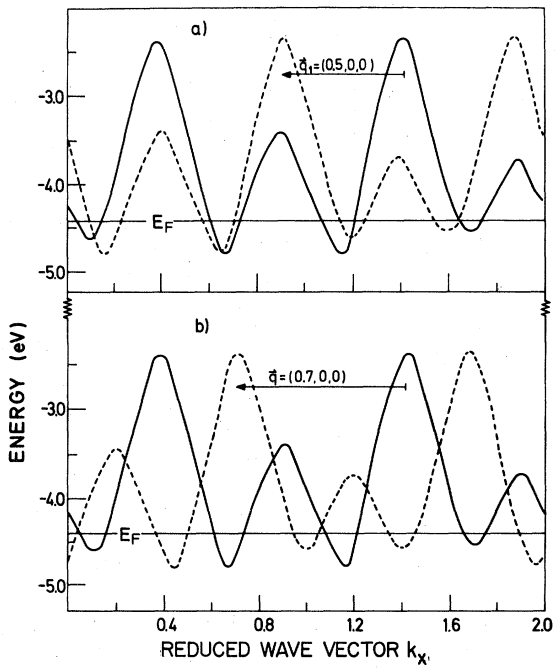

FIG. 11. Typical energy vs wave vector curves of band 3 solid lines depict $E_1(k)$ curves of Eq. (32), dashed lines represent the $E_2(k+y)$ curves of Eq. (33); $k = (0.15+x,\ 0.45,\ 0.05)$: (a) "normal" phonon $\vec{q} = (0.5, 0, 0)$; parallel bands, small $(v^x_k - v^x_{k'})$; (b) "anomalous" phonon $\vec{q} = (0.7, 0, 0)$; crossing of bands, large $(v^x_k - v^x_{k'})$.

same magnitude. We have found by detailed inspection of the contributions to $D_2^<(L)$ along $E_1(x)$ that in case (a), for $q=0.7$, all values were much larger than for $q=0.5$ [case (b)].

We summarize the above discussion:

(i) The requirements for the appearance of anomalies are different from the usual Fermi-surface anomalies in the Kohn-Overhauser[17] sense. The latter consider only the "bare" susceptibility, which may not even reproduce the right position in $\vec{q}$ space of the anomalous phonons.

(ii) The band structures favorable for anomalies are very anisotropic near E_F, with large dispersion in one (k space) direction and a small dispersion in the others. Consequently the Fermi surfaces have to be very anisotropic, e.g., a "jungle-gym" of interpenetrating rods as in the case of Nb.

(iii) The density of states $N(0)$ near E_F has to be sufficiently large, as in Nb, in order to provide enough scattering states. In materials with small $N(0)$, e.g., $Nb_{0.25}Mo_{0.75}$ (see Fig. 2), we would not expect much structure in the phonon dispersion.

(iv) Phonons with displacement fields parallel to small $(v_k^\alpha - v_{k'}^\alpha)$ behave very "normal," e.g., this is the case for $(0,0,0.5)L$, as well as for $(0,0,0.7)T$ in Nb.

We have investigated whether Eq. (29) is a sufficiently good approximation for the electron-ion form factors $g^\alpha_{k\mu,k'\mu'}$ to predict the positions of anomalies. Results for $D_2^<$ using Eq. (29) show good results for the anomaly along (ξ,ξ,ξ) at $\xi \approx 0.7$. However, there appear additional peaks at long wavelengths both for L and T. The latter stem from the fact that

$$\left\langle \sum_m A_m^*(\vec{k}) A_m(\vec{k}+\vec{q}) \right\rangle \approx 1 - cq^2$$

for $\vec{q} \to 0$ intraband scattering, with a large c, whereas $v^\alpha_{\vec{k}} - v^\alpha_{\vec{k}+\vec{q}} \propto q_\alpha$. These spurious peaks show the limitations of approximation Eq. (29) at long waves.

In Mo the very pronounced lowering of the phonons around the H point, including the crossing of L and T along (ξ,ξ,ξ) near $\xi \approx 0.9$, is caused by small energy interband scattering between bands 3 and 4, and 3 and 5, respectively. This is illustrated in Fig. 12 by a plot of $D_2^<(\vec{q})$. In $D_2^<$, also band 4 intraband scattering is included, but this term is only of minor importance. A very sharp peak of $D_2^<$ is observed both in L and T. Interestingly, the maximum is somewhat shifted, away from the H point to $\xi \approx 0.9$. We also note that $D_2^<(T) > D_2^<(L)$. In the phonon dispersion curves the off-center peak in $D_2^<$ does not generate a minimum near $\xi \approx 0.3$ because the $2nn$ force constant neutralizes it. The

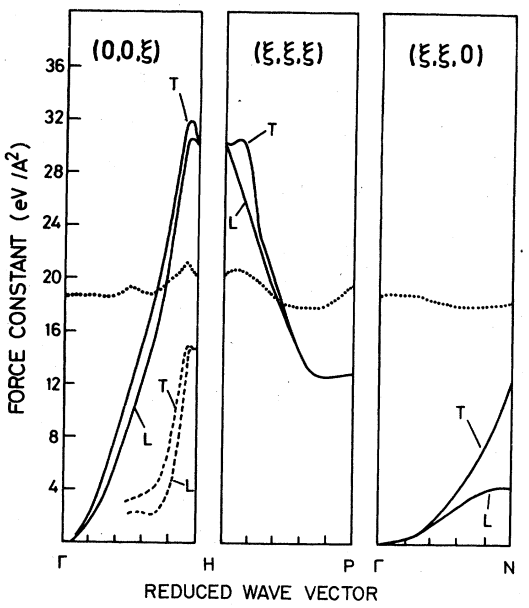

FIG. 12. $D_2^<$ contributions to the phonons in Mo. Solid lines represent full $D_2^<$ for L and T branches. Dotted lines show results for $\chi_{34,35}(q)$ in arbitrary units. Dashed lines represent approximation Eq. (31).

sharp structure of $D_2^<$ again originates from the very anisotropic band-structure topology near E_F, as illustrated in the complicated Fermi surface of Mo. Band 3 forms a holelike octahedron around the H point, while band 4 generates an electronlike octahedron around Γ of slightly smaller dimension. Because of the interaction of bands 4 and 5, the top pieces of the octahedron are cut off and the truncated octahedron is linked to the lenses situated around (0.5, 0, 0). The truncated top pieces of the octahedron reappear in the small Fermi surface pieces of band 5 near (0.3, 0, 0) (see Fig. 13).

Again, the electron-ion form factors strongly enhance the interband scattering between the states close to the two octahedral Fermi-surface pieces. This may have been expected from the fact that one of the octahedra is electronlike, the other holelike. Once more, we have verified the applicability of approximation Eq. (29) as compared to the constant matrix element approximation leading to $D_2(q) \sim \chi_0(\vec{q})$ (see Fig. 13). Once more we observe a strong anisotropy in the band dispersion, hardly any dispersion along the octahedral-surface triangles and very large dispersion in the direction normal to the triangular planes.

While in general the sharp structure in $D_2^<$ is caused by the electron-ion form factors, the small maximum in $D_2^<$ off H near $\xi = 0.9$ seems to be a typical Fermi surface singularity or Kohn anomaly. Indeed $\xi = 0.9$ corresponds precisely to a nesting

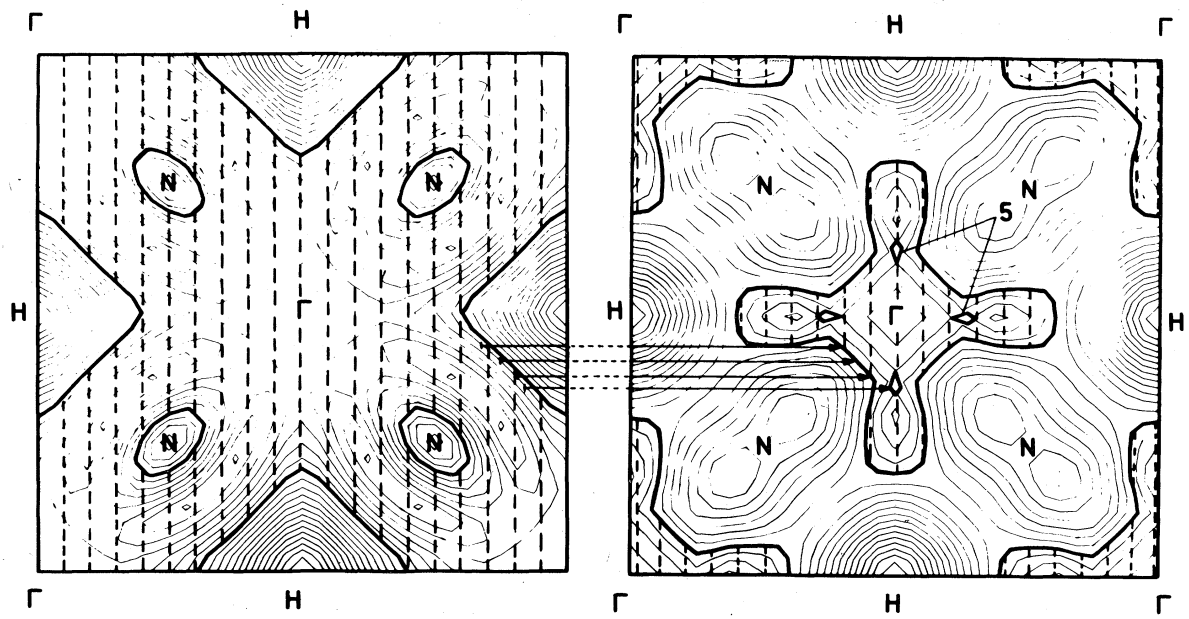

FIG. 13. Contour plots of band 3 and band 4 energy vs wave vector planes for Mo. The coordinates are the k_x and k_y directions; $k_z = 0$. The E_F contour lines are specially marked; all areas below E_F are indicated by hatching. The arrows indicate dominant scattering areas for the H point anomaly.

vector of the two octahedra, and the peak found in $\chi_0(q)$ is as pronounced as the D_2 peak.

Another interesting structure in the Mo dispersion curves is the lowering of the (T) mode N_3'. Similar to the H-point anomaly, yet not as pronounced, this lowering starts already in the Mo-rich alloys (see Fig. 9 of Ref. 6). We have found that it is essentially caused by interband scattering between bands 3 and 4, and is originating from a rather small area in the BZ. In this area the electron-ion form factors vary strongly in magnitude. This might cause convergence problems in our numerical integration, as mentioned above, and thus might explain the discrepancy with experiment, viz., the overestimation of the lowering both in the calculations for Mo and $Nb_{0.25}Mo_{0.75}$.

C. Short-range force constants

We have been concerned in this work with the anomalous features in the phonon spectrum and have simply parametrized the strong short-range constants. The short-range force constants give rise in the present work to the contributions D_0 and D_1 to the dynamical matrix. Some progress in understanding the short-range force constants has recently been achieved by Pettifor.[32] Pettifor's work is done in terms of angular momentum decomposition of wave functions about a given atom. He finds that the strongest short-range forces are due to the orthogonality of the d waves on a given atom with the tails of the waves from the other atoms which appear as s-p waves on the atom. The latter include the core s-p states on the other atoms as well as the d states on them. In our language these contributions are contained in D_1. However, we have been working extensively with the "valence" electronic states. To include the effects Pettifor has discussed, we would have to expand our tight-binding basis set to include some core states also and consider the overlap of such states on one atom with the valence states on its neighbors.

Because short-range force constants are primarily an orthogonality effect, they depend on the decay length of the atomic wave functions, as does, for instance, the electronic bandwidth. A relationship between the two is therefore expected and has been shown in a model calculation. The weak increase (about 20%) in the force constants from Nb to Mo, in fact, is of the same order as the increase in the electronic bandwidth.

D. Comparison with previous work

To explain the phonon anomalies, both phenomenological and semimicroscopic approaches have been employed. Weber[15] could account for the phonon anomalies in both transition metals and the transition-metal rock-salt compounds by a

double-shell model. The first shell was very much like the traditional shell model used for semiconductors, while the second shell was a new feature. The interaction between the second shells of next-nearest-neighbors was assumed of an attractive sign and led to most of the phonon anomalies. Doubtless this represents a parametrization of the term $D^{(2)}$ in the theory presented here.

More recently Allen[16] has presented a 16 parameter phenomenological theory which fits the experimental results well. The interatomic potentials are parametrized in terms of interactions between multipolar charge distributions around atoms. If one expands our term $D^{(2)}$ in terms of partial harmonics centered on different sites, one can understand Allen's phenomenology.

Gupta and Freeman[30] and Klein *et al.*[31] have calculated $\chi_0(q)$ for the transition-metal carbides and have found peaks at the position of the anomalies for intraband scattering. Similar calculations for the bcc transition metals reveal no peaks. In calculations using the present methods (to be reported later), the peaks in $D_2<(q)$ for transition-metal carbides are found to an order of magnitude higher than in $\chi_0(q)$ due to matrix-element effects.

Harmon and Sinha[13] and Hanke, Hafner, and Bilz[14] have used the inversion approach already described in Sec. V. Since this method is extremely unwieldy in dealing with TMC, they were forced to do model calculations. The model calculations yield some features of the phonon anomalies, but the physical reasons for the same anomalies are quite different in the two calculations. This is all the more surprising, considering the fact that identical expressions are used as a starting point in these calculations. At present it is not clear that the anomalies were not introduced in these calculations by hand through the choice of the models and of the parameters.

E. T_c and soft phonons

The superconducting transition temperature T_c for materials with similar shapes of phonon density of states is determined rather well[27] by the average phonon frequency $\langle\omega\rangle$, the Coulomb pseudopotential μ^* and the dimensionless parameter λ given by

$$\lambda = N(0)\langle I^2\rangle/m\langle\omega^2\rangle ,$$

where $N(0)$ is the density of states near the Fermi surface and $\langle\omega^2\rangle$ is approximately the mean-square phonon frequency. McMillan observed on the basis of experimental data that for transition metals and compounds, the product $N(0)\langle I^2\rangle$ varies much less than either $N(0)$ or $\langle I^2\rangle$. He therefore speculated that low $\langle\omega^2\rangle$, due say to phonon anomalies, leads to larger λ and hence to higher T_c (with a limit put by the prefactor $\langle\omega\rangle$ in front of the expression for T_c). This, together with the fact that within a given class of materials the one with the highest T_c has the biggest phonon anomalies, has led to an enormous literature discussing the inter-relationship of anomalies and high T_c.

A careful look[9] at the experimental results reveals that no such *causal* relationship exists. Among classes of transition metals $\langle I^2\rangle/m\langle\omega^2\rangle$ is a constant, so that λ within a given class varies simply as $N(0)$. According to the theory presented here, large parallel portions of Fermi surface in two directions in k space lead to increased magnitude of phonon anomalies. Such large parallel portions will generally occur only for flat bands in these two directions. Such flat bands (the "jungle-gym" Fermi surface) are responsible for the phonon anomalies in Nb and in some of the rock-salt transition-metal compounds. A correlation, and no more, therefore exists between phonon anomalies and high T_c.

The above is dramatically illustrated by comparing ZrN and ZrC. The former has a high T_c, $\approx$10 K and a huge-phonon anomaly; the latter has low T_c, $\lesssim$0.5 K and no phonon anomaly. $\langle I^2\rangle/m\langle\omega^2\rangle$ for the former is $\approx$2 eV, while for the latter it is $\approx$2.6 eV. The density of states is $\approx$0.12 eV/atom spins and $\approx$0.03 eV/atom spins, respectively.

ACKNOWLEDGMENTS

We wish to thank Dr. E. I. Blount and Dr. L. J. Sham for helpful conversations, and Dr. M. Schluter and Dr. P. Vashishta for providing some computer programs used in the calculations.

*Present address: Kernforschungs-zentrum, Karlsruhe, West Germany.

[1]B. M. Powell, P. Martel, and A. D. B. Woods, Phys. Rev. 171, 727 (1968).

[2]H. G. Smith and W. Glaser, Phys. Rev. Lett. 25, 1611 (1970); 29, 353 (1972).

[3]H. G. Smith, N. Wakabayashi, and M. Mostoller, in *Superconductivity in d- and f-Band Metals*, edited by D. H. Douglass (Plenum, New York, 1976).

[4]In Ref. 1, a Born–von Karman fit to the dispersion curves is made with force constants extending to 10 nearest neighbors.

[5]See for example, J. D. Axe, D. T. Keating, and S. C. Moss, Phys. Rev. Lett. 35, 530 (1975) and references therein.

[6]For a review, see F. J. DiSalvo and J. A. Wilson, Adv.

Phys. 24, 117 (1975).
[7]J. D. Axe and G. Shirane, Phys. Rev. B 8, 1965 (1973).
[8]S. D. Bader, S. K. Sinha, and R. N. Shelton, in Ref. 3.
[9]For a discussion of empirical relations between T_c and phonon anomalies, see C.M. Varma and R. C. Dynes in Ref. 3.
[10]See for instance, L. J. Sham, in *Dynamical Properties of Solids*, edited by G. K. Horton and A. A. Maradudin (North-Holland, Amsterdam, 1974).
[11]S K. Sinha, Phys. Rev. 169, 477 (1968).
[12]W. Hanke, Phys. Rev. B 8, 4585 (1973).
[13]S. K. Sinha and B. H. Harmon, Phys. Rev. Lett. 35, 1515 (1975).
[14]W. Hanke, J. Hafner, and H. Bilz, Phys. Rev. Lett. 37, 1560 (1976).
[15]W. Weber, Phys. Rev. B 8, 5082 (1973).
[16]P. B. Allen, Phys. Rev. 16, 5139 (1977).
[17](a) W. Kohn, Phys. Rev. Lett. 2, 393 (1959); (b) A. W. Overhauser, Phys. Rev. Lett. 4, 415 (1960).
[18]For a review, see J. Friedel, in *The Physics of Metals*, edited by J. M. Ziman (Cambridge University, Cambridge, 1969).
[19]W. E. Pickett and B. L. Gyorffy, in Ref. 3.
[20]C. M. Varma and W. Weber, Phys. Rev. Lett. 39, 1094 (1977).
[21]W. Kohn and L. J. Sham, Phys. Rev. 140, A1133 (1965).
[22]C. M. Varma, E. I. Blount, P. Vashishta, and W. Weber, Phys. Rev. B 19, 6130 (1979), referred to as I in the text.
[23]B. L. Gyorffy (private communication).
[24]L. F. Mattheiss, Phys. Rev. B 1, 373 (1970).
[25]J. R. Anderson, D. A. Papaconstantopoulos, J. W. McCaffrey, and J. E. Schirber, Phys. Rev. B 7, 5115 (1973).
[26]J. B. Diamond, in *Computational Methods in Band Theory*, edited by P. M. Marcus, J. F. Janak, and A. R. Williams (Plenum, New York, 1971), p. 347.
[27]W. L. McMillan, Phys. Rev. 167, 331 (1968).
[28]W. E. Pickett and P. B. Allen, Phys. Lett. A 48, 91 (1974).
[29]S. Guiliano, B.L. Gyorffy, R. Ruggeri, and G. M. Stocks, *Proceedings of the International Conference on Physics in Transition Metals, Toronto, 1977* (Institute of Physics, Bristol, London, 1978).
[30]M. Gupta and A. J. Freeman, Phys. Rev. Lett. 37, 364 (1976).
[31]B. Klein, D. A. Papaconstantopoulos, and L. L. Boyer, in Ref. 3; Solid State Commun. 20, 937 (1976).
[32]D. G. Pettifor, J. Phys. F 1, 613 (1977).